White-to-brown metabolic conversion of human adipocytes by JAK inhibition

Published in final edited form as:
Nat Cell Biol. 2015 January ; 17(1): 57–67. doi:10.1038/ncb3075.

White-to-brown metabolic conversion of human adipocytes by JAK inhibition

Annie Moisan[1], **Youn-Kyoung Lee**[2,3], **Jitao David Zhang**[1], **Carolyn S. Hudak**[2,3], **Claas A. Meyer**[1], **Michael Prummer**[1], **Sannah Zoffmann**[1], **Hoa Hue Truong**[1], **Martin Ebeling**[1], **Anna Kiialainen**[1], **Régine Gérard**[1], **Fang Xia**[2,3], **Robert T. Schinzel**[2,3], **Kurt E. Amrein**[1], and **Chad A. Cowan**[2,3]

[1] Roche Pharma Research and Early Development, Roche Innovation Center Basel, 124 Grenzacherstrasse, Basel, CH 4070, Switzerland. [2] Department of Stem Cell and Regenerative Biology and Harvard Stem Cell Institute, Harvard University, Massachusetts 02138, USA [3] Center for Regenerative Medicine, Massachusetts General Hospital, Boston, Massachusetts 02114, USA

Abstract

The rising incidence of obesity and related disorders such as diabetes and heart disease has focused considerable attention on the discovery of novel therapeutics. One promising approach has been to increase the number or activity of brown-like adipocytes in white adipose depots, as this has been shown to prevent diet-induced obesity and reduce the incidence and severity of type 2 diabetes. Thus, the conversion of fat-storing cells into metabolically active thermogenic cells has become an appealing therapeutic strategy to combat obesity. Here, we report a screening platform for the identification of small molecules capable of promoting a white-to-brown metabolic conversion in human adipocytes. We identified two inhibitors of Janus Kinase (JAK) activity with no precedent in adipose tissue biology that stably confer brown-like metabolic activity to white adipocytes. Importantly, these metabolically converted adipocytes exhibit elevated *UCP1* expression and increased mitochondrial activity. We further found that repression of interferon signalling and activation of hedgehog signalling in JAK-inactivated adipocytes contributes to the metabolic conversion observed in these cells. Our findings highlight a novel role for the JAK/

Correspondence and requests for materials should be addressed to Annie Moisan and Chad Cowan. Contact: chad_cowan@harvard.eduannie.moisan@roche.com.

Author contributions: A.M. designed and performed experiments, analyzed data and wrote the manuscript; Y-K.L. performed experiments, analyzed data and edited the manuscript; R.G., C.S.H. and F.X. performed experiments; J.D.Z. and M.E. performed bioinformatics analyses and contributed to main text related to figure 7; H.H.T., S.Z. and M.P. performed high content imaging analysis; A.K. performed RNA sequencing; C.A.M. and R.T.S. supervised stem cell activities; K.E.A. supervised the project and C.A.C. supervised the project and wrote the manuscript. A.M., Y-K.L., R.G., C.H., M.P., J.D.Z., H.H.T., S.Z. and A.K. contributed to description of online methods.

AUTHOR INFORMATION

Primary accession number

RNA sequencing data set generated in this study is available online at NCBI GEO, Accession Number GSE57896.

Competing financial interests

The authors declare no competing financial interests.

Primary Accession Numbers

RNA sequencing data set generated in this study is available online at NCBI GEO, Accession Number GSE57896.

STAT pathway in the control of adipocyte function and establish a platform to identify compounds for the treatment of obesity.

Mammals possess two distinct types of adipose tissue: white and brown fat. White adipose tissue (WAT) stores excess energy and has a number of endocrine functions such as regulating satiety via leptin secretion. In contrast, brown adipose tissue (BAT) maintains body temperature via non-shivering thermogenesis. BAT releases energy in the form of heat by uncoupling the respiratory chain via uncoupling protein 1 (UCP1). In addition to thermogenesis, BAT activation in rodents accelerated plasma clearance of triglycerides, ameliorated insulin resistance and protected against obesity[1, 2]. Recently, PET/CT imaging revealed adipose tissue with thermogenic activity and UCP1 expression in human adults[3]. These studies also found that BAT is inversely associated with adiposity, high body mass index and hyperglycemia. Based on these findings, there has been an increased interest in BAT as a therapeutic target to treat metabolic disorders.

Mouse studies have reported the emergence of UCP1-expressing cells in WAT upon cold exposure, β-adrenergic stimulation and peroxisome proliferator-activated receptor gamma (PPARG) activation[4-10], a phenomenon referred to as browning. These brown-like cells arise from the recruitment of specific precursor cells[11] and/or the conversion of white into brown-like cells[12]. Two human trials have also demonstrated de novo generation of brown adipocytes upon cold acclimation combined with increased non-shivering thermogenesis and decreased body fat mass[13, 14]. These studies suggest identifying inducers of browning in humans may ameliorate obesity related diseases. To this end, we established a screening platform to discover small molecules capable of promoting white-to-brown metabolic conversion in human adipocytes and identified Janus kinase (JAK) inhibitors as molecules with browning potential. In addition, we show that human pluripotent stem cell-derived adipocytes provide a scalable, robust and reliable cell model for adipocyte browning studies, compound screening and drug discovery.

RESULTS

A screening platform for adipocyte browning identifies inducers of *UCP1*

We used a human pluripotent stem cell (PSC)-derived adipocyte model to study the pharmacological conversion of white to brown-like adipocytes. In this approach, adipocytes are obtained via the inducible expression of transcription factors in PSC-derived mesenchymal progenitor cells (MPCs) and the addition of an adipogenic cocktail to the media[15]. Inducible expression of peroxisome proliferator-activated receptor gamma2 (*PPARG2*) alone or a combination of *PPARG2*, CCAAT/enhancer-binding protein beta (*CEBPB*) and PR domain containing 16 (*PRDM16*) drives cell differentiation towards the white (PSC-WA) or brown (PSC-BA) lineage respectively[15]. We reasoned that *CEBPB* and *PRDM16* could be replaced by small molecules to direct *PPARG2*-expressing MPCs towards a brown-like phenotype (Fig. 1a). We monitored the responsiveness of PSC-WA to known modulators of *UCP1* expression[16] and observed up-regulation of *UCP1* mRNA levels upon treatment with forskolin, 3-isobutyl-1-methylxanthine (IBMX), rosiglitazone

and bone morphogenic protein 7 (BMP7), validating the use of PSC-WA for browning assays (Supplementary Figure 1).

Utilizing this model we established a screening assay for assessing the conversion of white to brown-like adipocytes (Figure 1b). A focused library of 867 small molecules that has a large degree of activity annotation, facilitating deconvolution of mechanism of action was applied at day 7, when cells are differentiating and will adopt a white phenotype if no additional stimulus is applied. Adipocytes were exposed to compounds for 7 days and collected at day 14 for analysis. As a browning index, *UCP1* expression was monitored by *UCP1* mRNA capture plates followed by branched DNA amplification. Expression of fatty acid binding protein 4 (*FABP4*), an adipocyte specific gene, served as internal control to eliminate anti and pro-adipogenic compounds not specific to *UCP1*, such as the PPARG agonist rosiglitazone (Fig. 1c, red dot). Out of 135 *UCP1* inducers (see online methods for statistical analysis), 52 compounds induced both *UCP1* and *FABP4* levels (Fig. 1c, blue dots). Among the 83 compounds that induced *UCP1* specifically (Fig. 1c, green dots), compounds that induced *UCP1* at least 2 fold were selected as browning hits and compared to rosiglitazone-like compounds in an independent experiment (Fig. 1d and Supplementary Table 1). *UCP1* induction by thyroid hormone receptor beta (THRB) agonists and phosphodiesterase enzyme 3 (PDE3) inhibitors is in accordance with previously reported up-regulation of *UCP1* promoter activity by thyroid hormone and cAMP[17-20]. Of particular interest, three annotated inhibitors of Spleen Tyrosine Kinase (SYK) and two inhibitors of Janus Kinase 3 (JAK3) showed the highest *UCP1*/*FABP4* ratio. JAK3 and SYK are best characterized for their role in immune cells development and physiology and as mediators of pro-inflammatory pathways[21]. Recently, the JAK-STAT pathway was found to modulate early adipogenesis upstream of PPARG but little evidence supported a role in adipose tissue remodeling and thermogenicity[22].

A subset of *UCP1*-inducers modulate adipocyte lipid droplet morphology

White adipocytes have a single or a few large lipid droplets, whereas the brown adipocytes contain multiple small lipid droplets. We exploited this morphological difference to evaluate the browning effects of newly identified *UCP1*-inducer compounds. Following treatment of PSC-WA with selected compounds (Fig. 1b), we used fluorescent dyes to mark nuclei and lipid droplets, and performed high content imaging to quantify the number and size of lipid droplets per cell. After 7 days of treatment with selected JAK3 and SYK inhibitors, we observed changes in lipid droplet morphology that are typical of brown-like adipocytes (Fig. 2a). Contrastingly, a THRB agonist was inert in this assay despite elevation of *UCP1* expression (Fig. 2a and 1d). We determined the lipid area of small ($<1070\mu m^2$) and large ($>1070\mu m^2$) droplets per well (Fig. 2b, curve graphs) and used the ratio small/large droplet area as a 'brown-like lipid index' for each compound, as exemplified in Figure 2c for DMSO, JAK3 inhibitor, SYK inhibitor and THRB agonist. A total of 39 compounds that induced *UCP1* or displayed visible effects on lipid morphology during the browning screen were thereby quantified and ascribed a brown-like lipid index (Fig. 2d, Y-axis). When the two browning indices were taken into account, i.e. *UCP1*/*FABP4* and lipid droplet morphology, JAK3 and SYK inhibitors were the most potent browning compounds from our screen (Fig. 2d). In addition, this analysis revealed that brown-like lipid morphology was

poorly correlated with elevated *UCP1* expression, indicating that quantification oflipid droplet size is not a suitable phenotypic readout for adipocyte browning, at least in our system.

Validation of tofacitinib and R406 browning compounds in primary adipocytes

As model browning compounds, we selected the JAK3 inhibitor tofacitinib and the SYK inhibitor R406 for their potency in our browning assay and for their clinical relevance (Supplementary Figure 3). We examined the dose-response of tofacitinib and R406 in PSC-WA and found that the *UCP1/FABP4* ratio reaches a plateau at 2 μM for tofacitinib and 1 μM for R406 (Fig. 3a). Graphical representation of *UCP1* and *FABP4* normalized on housekeeping gene revealed a *UCP1*-specific effect of tofacitinib, while R406 induced both *UCP1* and *FABP4* expression when dosed above 1 μM (Fig. 3a). We confirmed that tofacitinib and R406-mediated increases in *UCP1* mRNA levels translated into accumulation of UCP1 protein (Fig. 3b) and observed concomitant elevation in PRDM16 protein (Fig. 3b).

Importantly, we validated the effects of tofacitinib and R406 on *UCP1* and *FABP4* expression in lentiviral-free, human primary adipose tissue-derived stem cells (ADSCs) differentiated according to standard procedures (Fig. 3c). Tofacitinib and R406 also caused the emergence of brown-like lipid droplet morphologies in ADSC-derived adipocyte cultures and appeared superior to BMP7 in this assay (Fig. 3d). Finally, we subjected mouse white adipose tissue explants to increasing doses of tofacitinib and R406 and observed up-regulation of *UCP1* expression in explants of sub-cutaneous, but not visceral, origin (Fig. 3e and Supplementary Figure 4).

Tofacitinib and R406 block the JAK-STAT1/3 pathway during adipocyte browning

Tofacitinib is a potent inhibitor of signaling through JAK1 and JAK3 with 5-100 fold selectivity over JAK2 in cell-based assays[23, 24]. R406 is described as a potent and specific SYK inhibitor, but also targets JAKs, c-kit, Lck, and FLT3 when profiled at 2 μM[25]. We sought to determine the pharmacological signature of tofacitinib and R406 in human adipocytes where target abundance and signaling activity might differ from immune cells. First we used RNA sequencing analysis of PSC-WA to evaluate the abundance of known targets of tofacitinib and R406. JAK1 was the most abundantly expressed member of the Janus kinase family, followed by Tyk2, JAK2 and JAK3 (Figure 4a). The abundance of SYK, c-kit, Lck and FLT3 was below statistical significance suggesting that R406 may exert its browning effect via JAK inhibition.

To profile possible downstream targets, PSC-WA were treated with tofacitinib and R406 at the determined ‘browning dose’ (2 and 1 μM respectively) for 20 minutes and screened by reverse phase protein array (RPPA) covering 51 different phospho-isoforms. RPPA analysis revealed STAT3 as the main downstream target for both tofacitinib and R406 (Supplementary Figure 5). While the effect of tofacitinib was restricted to STAT3 in the RPPA panel, R406 had additional downstream targets including AKT, EGFR and ERK1/2 (Supplementary Figure 5). We further investigated the effect of tofacitinib and R406 on JAK/STAT, AKT and ERK1/2 pathways by immunoblot analysis. As shown in Figure 4b,

tofacitinib and R406 blocked tyrosine phosphorylation of STAT1 and STAT3 after 20 minutes, an effect that is exacerbated upon 7 days of treatment. In a dose response experiment, the gradual increase in UCP1 levels negatively correlated with STAT3 phosphorylation (Fig. 4c). Noticeably, STAT1 protein level decreased after treatment with tofacitinib and R406. Tofacitinib had no effect on AKT and MAPKs, whereas R406 significantly decreased the phosphorylation level of AKT, ERK1 and ERK2 (Fig. 4b). AKT phosphorylation was restored at day 7, suggesting an adaptive response to maintain adipocyte homeostasis and insulin signaling. Phospho-STAT5 was undetectable in our assay and p38 and JNKs were unaltered at both times. Thus, JAK inhibitors likely change *UCP1* expression via a different route than the cAMP/p38 pathway downstream of β3-adrenergic stimulation[26, 27].

Tumor necrosis factor alpha (TNF-α) represses *UCP1* expression in brown adipocytes[28], an effect also observed in PSC-WA (Fig.4d). Since TNF-α can signal through JAK/STAT and ERK pathways, we tested CP-690550 and R406 ability to antagonize TNF-α repression of *UCP1* expression. CP-690550 and R406 partially and fully restored *UCP1* levels respectively, in agreement with the JAK/STAT-specific and JAK/STAT-ERK1/2 effects of each compound (Fig.4b). In addition, the combination of CP-690550 and R406 was not superior to R406 alone in increasing *UCP1* expression (Fig.4e), supporting evidence that CP-690550 and R406 functionally overlap.

Finally, we tested Ruxolitinib, a JAK1/2 inhibitor, and observed up-regulation of *UCP1* expression without significant regulation of *FABP4* with concomitant inhibition of STAT1/3 phosphorylation (Fig. 4f). Three other JAK1/2 inhibitors, AZD1480, CYT387 and Baricitinib, also showed up-regulation of *UCP1* expression (Fig. 4g). A combination of tofacitinib and Ruxolitinib did not further increase *UCP1* expression (Fig. 4h, left panel), unlike a combination of tofacitinib with a THRB agonist (Fig. 4h, right panel). Altogether, the data highlight a central role for the JAK1/2-STAT1/3 pathway in *UCP1* expression in adipocytes.

Progressive and stable conversion of adipocytes by JAK inhibition

Molecules that increase *UCP1* expression by directly activating the *UCP1* promoter[26] may not be suitable for *in vivo* induction of browning or therapeutically useful to combat obesity. Alternative mechanisms of browning such as adipocyte metabolic remodeling are needed, and our screening platform was designed for this purpose. We examined the kinetics of tofacitinib and R406-mediated browning in comparison to THRB agonist, which also ranked in the top-10 best *UCP1* inducers but failed to modify lipid droplet morphology (Fig. 1d and 2). The *UCP1* promoter contains a thyroid hormone responsive element (TRE)[20] and as expected, a THRB agonist rapidly increased *UCP1* levels (Fig. 5a). Contrastingly, *UCP1* mRNA levels increased more slowly and progressively in tofacitinib and R406-treated adipocytes (Fig. 5a), consistent with remodeling of cellular metabolism rather than direct modulation of *UCP1* promoter activity.

If a stable white to brown-like conversion is achieved via JAK inhibition, the brown-like phenotype should persist upon removal of CP-690550 and R406. To test this, we selected 9 inducers of *UCP1* mRNA levels from the original screen and treated PSC-WA with each

compound for 7 days, washed with compound-free medium, and maintained in compound-free medium for an additional 14 day-period (Fig. 5b). Remarkably, all cells pre-treated with JAK inhibitors displayed high levels of *UCP1* mRNA and reduced lipid droplet size at day 28 compared to DMSO-treated cells while all other compounds lost their browning effect after washout (Fig. 5b-c). Finally, we repeated the washout experiment with tofacitinib and R406 and added TNF-α at day 26, 48 hours prior to cells collection. Even in the absence of compounds, adipocytes pre-treated with tofacitinib and R406 maintained higher level of *UCP1* when challenged with TNF-α (Fig. 5d). Altogether, these results indicate that JAK inhibition leads to the stable acquisition of brown-like metabolic properties in human adipocytes.

JAK-inactivated adipocytes acquire a brown-like metabolic program

Brown adipocytes are characterized by high mitochondrial content as well as high metabolic activity[1]. Mitochondrial content was assessed by determining the ratio of subunit I of Complex IV (COX-I), which is mitochondrial DNA-encoded, on the 70kDa subunit of Complex II (SDH-A), which is nuclear DNA-encoded. Quantification of COX-1 and SDH-A immunoblots showed a significant up-regulation of mitochondrial content in R406 and tofacitinib-treated PSC-WA and ADSC adipocytes (Fig. 6a). To determine the impact of these changes on metabolic activity, oxygen consumption rate (OCR) was measured. We found that basal, uncoupled and maximal respiration were increased when PSC-WA and ADSC adipocytes were pre-treated for 7 days with tofacitinib or R406 as compare to a DMSO control (Fig. 6b). Thermogenesis in brown adipocytes is fuelled by lipid catabolism, which can be measured by release of glycerol from fatty acid. We quantified the level of free glycerol from adipocyte culture medium and observed a ~2.5 fold increase of basal lipolysis in tofacitinib and R406-treated adipocytes (Fig. 6c), but no significant increase in forskolin (FSK) stimulated lipolysis (Fig. 6c). Altogether, these data suggest the engagement of a brown-like metabolic program upon inhibition of JAK/STAT in human adipocytes.

JAK-inactivated adipocytes maintain a white adipocyte transcriptional identity

To determine whether tofacitinib and R406 treatment had converted the transcriptional identity of white adipocytes, we performed RNA sequencing and analyzed the whole transcriptome of MPC, PSC-WA, PSC-BA and compound-treated PSC-WA. We used multidimensional scaling to project expression data, where distances between samples reflect the differences between global gene expression profiles. As expected, PSC-WA and PSC-BA moved away from undifferentiated PSC-MPC, and away from each other (Fig. 7a). Despite the acquisition of a brown-like metabolic profile, tofacitinib and R406-treated PSC-WA global expression profiles clustered with untreated PSC-WA samples and not with PSC-BA (Fig. 7a). Consistent with our findings, RNAseq analyses revealed a strong induction of *UCP1* expression by tofacitinib and R406 (Fig. 7b). Among known positive regulators of brown adipogenesis, R406 promoted mRNA expression of *PGC1α*, *PGC1β* and *PPARG* (Supplementary Figure 6). Intriguingly, PRDM16 mRNA expression was decreased in treated-PSC-WA despite an increase at the protein level (Supplementary Figure 6 and Fig. 3). These data indicate that adipocyte browning by JAK inhibition occurs by functionally remodelling white adipocytes and through the acquisition of brown-like metabolic activities rather than via cell fate conversion.

Downregulation of IFN and activation of hedgehog signaling contribute to metabolic browning downstream of JAK inhibition

To decipher the molecular mechanisms underlying metabolic browning of adipocytes via JAK inhibition, gene set analyses were performed and enrichment scores calculated for 9116 gene sets. Strikingly, all gene sets altered by tofacitinib were down-regulated, most prominently interferon (IFN) response (IFNα/β/γ), STAT1/3/5 pathway and pro-inflammatory pathways (OSM and IRF) (Fig. 7c). Similarly, R406 largely attenuated IFN response and mediators of inflammation (OSM, TNF, chemokine) (Fig. 7c). Tofacitinib and R406 treated adipocytes closely resembled one another in the differential expression profiles of IFN targets, of which 25 genes where nearly equally regulated by the two inhibitors (Fig. 7d and e). IFNα/β/γ bind to JAKs and activate STAT1/2/3[29]. Thus the gene set enrichment score confirm our findings that tofacitinib and R406 inhibit the JAK-STAT pathway in adipocytes. The transcriptional changes downstream of R406 displayed a broader spectrum of regulated gene sets in comparison to tofacitinib including up-regulation of PPARG, SREBF and BMP target genes (Fig. 7c and Supplementary Figure 6), an observation in accordance with its positive effect on *FABP4* expression (Fig. 3a).

We further interrogated RNAseq data for individual genes up-regulated in both tofacitinib and R406-treated PSC-WA. 54 genes were up-regulated by both compounds, 17 of which were BAT-specific (Supplementary Figure 6). Notably, we observed that GLI1 was up-regulated in tofacitinib and R406-treated PSC-WA and in PSC-BA (Fig. 7f). Moreover, three GLI1-target genes, *SFRP5*, *KLHL31* and *SHH*, were up-regulated, suggesting activation of sonic hedgehog (SHH) signalling downstream of JAK/STAT inhibition during adipocyte browning.

The common gene signature of tofacitinib and R406-treated PSC-WA suggests that inhibition of JAK/STAT signaling short-circuits the IFN/JAK/STAT positive feedback loop and thereby progressively alleviates anti-browning and/or activates browning signals. We verified this hypothesis by inducing a white phenotype after addition of IFNγ to PSC-WA, observable by the formation of unilocular lipid droplets, an effect that was reversed by addition of tofacitinib or R406 (Fig. 8a). Moreover, IFNγ treatment of PSC-WA and PSC-BA decreased the *UCP1/FABP4* ratio and increased expression of the white adipocyte marker HSL (Fig. 8b).

We observed that repression of IFN response was followed by up-regulation of BA-specific transcripts in tofacitinib and R406-treated PSC-WA including the GLI1 transcription factor (Fig. 7f). The previously reported antagonistic link between IFN and SHH[30] prompted us to evaluate the functional relevance of up-regulation of GLI and GLI-target genes in tofacitinib and R406-mediated metabolic browning. To examine the contribution of SHH signalling downstream of JAK/STAT inhibition during metabolic browning of adipocytes, PSC-WA were subjected to increasing doses of cyclopamine, a SHH pathway inhibitor, in combination with DMSO, tofacitinib or R406 for 7 days. Addition of cyclopamine did not significantly alter gene expression in DMSO-treated PSC-WA but completely blocked tofacitinib-mediated induction of *UCP1* expression (Fig. 8c). Interestingly, high doses of cyclopamine antagonized the effect of R406 on *UCP1* expression but did not block the

induction of *FABP4*, thereby decoupling the regulation of *UCP1* and *FABP4* by R406 (Fig. 8c). The up-regulation of PPARG activity by R406 (Supplementary Figure 6) likely accounts for this observation. *UCP1* expression was also down-regulated in PSC-BA upon treatment with cyclopamine (Supplementary Figure 7). These results support a role for SHH signaling in the acquisition of brown-like properties in human adipocytes.

Overall, we provide evidence that inhibition of JAK down-regulates interferon signaling in human adipocytes. The persistent repression of IFN signaling relieves inhibition of the SHH pathway[30] and thereby contributes to the upregulation of *UCP1* and promotes the metabolic browning of adipocytes (Fig. 8d).

DISCUSSION

The remarkable phenomenon of adipocyte browning –or the emergence of brown-like adipocytes in white adipose depots– and its associated metabolic benefits has spurred interest in the discovery of pharmacotherapies targeting adipose tissue to treat metabolic diseases such as obesity and type 2 diabetes. Here, we established a small molecule screen to unravel pharmacologically accessible pathways capable of inducing a brown-like thermogenic program in human adipocytes. We identified tofacitinib and R406 as potent inducers of *UCP1* and via secondary screening established their role in remodeling lipid droplet morphology in human adipocytes. We found that both compounds target the JAK-STAT1/3 pathway in adipocytes and have a distinct progressive and long-lasting effect that confers brown-like metabolic properties to white adipocytes. Our results further highlight important antagonistic interplays between interferon and sonic hedgehog signaling in adipocyte function.

Our findings are in line with previously proposed functions of Hedgehog in determining white versus brown adipose cell fate[31]. By using the Hedgehog activator Smoothened Agonist (SAG) in various mouse cell lines, Pospisilik *et al.* showed that activation of Hedgehog blocks white, but not brown, adipocyte differentiation and solely in the absence of cAMP and glucocorticoid signaling. In our study, activation of Hedgehog signaling by JAK inhibition occurred in *PPARG2* expressing cells in the presence of cAMP and glucocorticoid signaling and promoted the acquisition of a brown-like metabolic phenotype. It is thus conceivable that activation of Hedgehog signaling after adipogenesis is initiated and during the maturation of white adipocytes may promote the acquisition of brown-like properties. We further demonstrated that pharmacological inhibition of Hedgehog decreased *UCP1* expression in genetically programmed BA and brown-like adipocytes. Interestingly, Pospisilik *et al.* reported the up-regulation of *UCP1* mRNA levels in WAT and BAT tissue upon genetic activation of Hedgehog in the aP2-SufuKO mouse, reminiscent of the data presented here upon treatment with tofacitinib and R406. More recently, an antagonistic crosstalk between Hedgehog and IFNγ in white adipose tissue has been described, wherein inhibition of Hedgehog signaling by IFNγ rescues white adipocyte differentiation[30]. Our findings further reinforce and refine the role of an IFN-JAK/STAT-SHH axis in human adipocyte biology. A recent study by Derecka *et al*. revealed a positive role for Tyk2 and Stat3 in the regulation of $Myf5^{+}$ pre-adipocyte differentiation and BAT development in mice[32]. In light of our findings, it will be interesting to investigate the role of TYK2/STAT3

and other JAK/STATs in committed, functional brown adipocytes. A fine tuning of the JAK/STAT pathway at various stages of differentiation and maturation might be key for optimum BAT expansion and metabolic function.

The utility of JAK inhibition as a therapeutic for obesity is complicated by the well-described role of this signalling pathway in the immune system. In fact, tofacitinib is currently approved in the United States to treat rheumatoid arthritis. Thus, if one were to envision targeting adipose tissue by *in vivo* administration of an IFN/JAK/STAT inhibitor or similar compound it would almost certainly need to be delivered locally and prevented from spreading systemically or alternatively targeted selectively to white adipocytes. One could also conceive of a cell-based therapy wherein JAK inhibition of patient-derived adipocytes *ex vivo* is followed by transplantation to treat obesity, but this therapeutic modality would need to overcome numerous and significant obstacles before becoming a reality. A further limitation of the current study is the lack of evidence that JAK inhibition would promote metabolic browning *in vivo*, in particular in humans were evidence supporting this phenomenon is scant. Thus, additional research is required before inhibition of IFN/JAK/STAT signalling could be utilized therapeutically for the treatment of metabolic disorders.

Recent progress in the development of human embryonic stem cells and induced pluripotent stem cell -based models of disease have delivered unprecedented tools for basic research and translational medicine. However, their applicability for drug discovery remains to be fully realized. Here, we tested the suitability of a human PSC-derived adipocyte model[15] for screening and functional browning assays. We found this model provided an inexhaustible and rapidly expandable source of human adipocytes for screening and downstream assays. Moreover, it proved easily scalable and highly reliable in our screening assay. The responsiveness of human PSC-derived adipocytes to known and newly identified browning molecules closely mirrored that of primary adipose derived stromal cells (ADSC) further validating this model for adipocyte cell fate and browning studies.

To conclude, we successfully performed a proof of concept screen utilizing an innovative stem cell-based model to identify compounds that convert human adipocytes to metabolically active brown-like cells. Given that this platform is amenable to very high-throughput screening it has considerable potential to contribute to the discovery of novel biological modulators of adipocyte cell fate and function and possibly to the development of new drugs for patients with metabolic disorders.

METHODS

Maintenance of human MPCs and ADSCs and differentiation into adipocytes

MPCs, white adipocytes (PSC-WA) and brown adipocytes (PSC-BA) were generated and differentiated as described by Ahfeldt *et al.*[15] with the following modifications: MPCs were derived from human embryonic stem cell line SA001 (Cellartis), MPCs were seeded at 75% confluency in 15 cm dishes, incubated overnight with lentiviral particles at an MOI of 50 for each virus and maintained in growth medium without virus for 24 hours. Infected MPCs (herein PPARG2-MPCs) were counted and seeded in 96 well plates at a density of 37 500 cells/cm^2 in growth medium. The next day (Day 0), growth medium was changed for

induction medium consisting of adipocyte medium (DMEM, Knockout Replacement Serum, non-essential amino acids, insulin, dexamethasone) supplemented with 700 ng/ml doxycycline and 0.5 μM rosiglitazone. 72 hours later (Day 3), induction medium was replaced by differentiation medium (adipocyte medium supplemented with 700 ng/ml doxycycline) for 96 hours. From day 7, white (PSC-WA) and brown (PSC-BA) adipocytes were maintained in adipocyte medium and refreshed every two or three days.

Adipose tissue-derived stem cells (ADSCs) were obtained from PromoCell (human mesenchymal stem cell from adipose tissue or hMSC-AT, catalog number C-12977) and maintained in mesenchymal stem cell growth medium (PromoCell C-28010) according to manufacturer's instructions. For differentiation studies, ADSCs were seeded in 96 well plates at a density of 37 500 cells/ cm^2. At 90% confluency, growth medium was changed for adipogenic differentiation medium (PromoCell C-28011) and refreshed every third day.

Compound library for adipocyte browning screen

A library of 867 small molecules of known mode of action was assembled by combining Roche internal reference compounds and commercially available screening libraries (Tocriscreen Collections #3514 Kinase inhibitor toolbox, Selleckchem Stem cell #L2100, Selleckchem Epigenetic #L1900 and Selleckchem GPCR #L2200). All compounds were pre-dissolved in DMSO, diluted to 5mM stock solutions and stored at -80°C. A list of compounds ID, mode of action and CAS numbers is available upon request.

Browning screen, statistical analysis and hit validation

PPARG2-MPCs were seeded in 96-well plates, induced and differentiated into PSC-WA as described above. A library of small molecules was applied at a 5 μM final concentration in biological duplicates at day 7, 10 and 12 in fresh adipogenic medium. DMSO and rosiglitazone (0.5 μM final concentration) were included on each plate as negative and positive controls respectively. Adipocytes were collected at day 14 and processed for *UCP1* and *FABP4* mRNA analysis by bDNA.

For statistical analysis, the raw mRNA signal was log-transformed and normalized to fold-change of the per plate median of the negative controls for all calculations, $x_{norm} = \log(s_{raw})/M_{neg}$, where $M_{neg} = median_{plage}\{\log(s_{neg})\}$. The data quality was assessed by calculating the Z' factor based on positive and negative controls for each plate (Supplementary Figure 1b). For UCP1, <Z'> = 0.50, and Z' > 0.50 for 11 out of 24 plates; for FABP4, <Z'> = 0.64, and Z' > 0.50 for 18 out of 24 plates. This is characteristic for a good quality HCS[34]. To evaluate the replicates performance, biological duplicates were aggregated to their mean; 5% of the compounds were excluded from further analysis since their *UCP1* difference was larger than 0.07; Supplementary Figure 1c shows that the replicate difference distribution is constant over the entire range, suggesting a constant replicate variance.

The remaining 832 compounds were used for hit selection as described before[35]. Knowing the constant variance from the controls, a p-value could be assigned to each compound following the test statistics $T = (x_{norm} - 1)/\sigma_{neg}$, where $\sigma_{neg} = MAD_{plate}\{\log(s_{neg})\}$,

$x_{norm}(M_{neg}) = 1$, which is normal distributed for inactive compounds (i.e., under the null hypothesis H_0). We next estimated the false discovery rate (FDR) by p-value distribution analysis[36] and applied a selection threshold of <0.01. Supplementary Figure 1d, left panel, illustrates the selected primary actives among the non-selected compounds in a quantile-quantile plot and the p-value distribution (inset). Next, a second hit selection process for *FABP4* was included, again at a FDR cutoff <0.01 (Supplementary Figure 1d, right panel). We thereby found 135 *UCP1* hits, of which 52 were assigned as "Rosiglitazone-like" compounds that induced both *UCP1* and *FABP4*. In the validation experiment, we selected browning hits that induced *UCP1* by at least two fold and *UCP1/FABP4* by at least 1.5 fold. PPAR agonists were also included for a total of 33 re-tested compounds, of which 26 were confirmed (Supplementary Figure 1d, left panel). 15 validated hits and PPAR agonists are displayed in figure 1d and chemical names are provided in Supplementary Table 1.

High content imaging

At day 14 of browning assay, cells were fixed with 4% Paraformaldehyde in PBS for 15 minutes at room temperature, incubated with blocking buffer (5% Donkey Serum, 0.5% triton X-100 and 0.02% Azid NaN3 in PBS) for 30 minutes at RT and stained with 10 μM Hoechst [B2261, Sigma] and 20ng/ml of Bodipy ® 493/503 (D-3922, Life technologies) in PBS for 30 minutes at room temperature. Samples were kept in PBS. Fluorescence Images where acquired using the Opera QEHS reader (Perkin-Elmer, Hamburg, Germany) equipped with a Nipkow Spinning disc for confocality using a 20× objective. Hoechst stain was imaged with laser excitation at 405nm laser and a 455/70nm band path filter for emission. The lipid stain was imaged using laser excitation at 488nm, and a 535/60nm / BP filter for emission. The image segmentation was done with the instrument integrated software Acapella. A custom made algorithm was used to identify the morphologically heterologous nuclei in the mixed cell population: Larger, round and relatively dark (brown adipocytes, non-differentiated cells); smaller, bright, more irregular shaped nuclei (white). The lipid droplets were segmented independently as either larger round bright objects or darker spots and assigned to individual nuclei based on an equidistant ring around the nuclei. The ratio in the total area of cell related droplets above and below 1070 μm^2 was quantified as shift between a more white and brown phenotype in the whole cell population. Cell classification; Adipocyte: total droplet area above 750 μm^2 and/or >10 spots <50 μm^2. White subtype: Minimum one droplet above 830 μm^2, brown subtype: No larger droplets, minimum 10 spots.

Browning assay with tofacitinib, R406, JAK inhibitors and BMP7

Following screening and hit validation, browning assays were performed with commercially available JAK3 inhibitor (tofacitinib, Selleckchem S5001) and SYK inhibitor (R406, Selleckchem S1533). PSC-WA and ADSCs were differentiated and treated following the assay design of the browning screen. Tofacitinib was added at 2 μM and R406 at 1 μM final concentration unless otherwise indicated on figures and legends. THRB agonist (CAS 219691-94-8) was added at 5 μM final concentration. Ruxolitinib (Selleckchem S1378), Baricitinib (Selleckchem S2851), CYT387 (Selleckchem S2219) and AZD1480 (Selleckchem S2162) were added at 0.1-5 μM final concentration as indicated on figures.

Recombinant human BMP7 (R&D systems, 354-BP) was added at 10 ng/ml final concentration in adipogenic medium supplemented with 250 μM IBMX (3-Isobutyl-1-methylxanthine, Sigma-Aldrich I7018) at day 0, 3 and 5. In ADSCs, BMP7 was added at 10 ng/ml at day 7, 10 and 12. Tofacitinib and R406 were added following the same conditions as BMP7 for proper comparison.

Browning of mouse adipose tissue explants

Subcutaneous and visceral adipose depots were dissected from 8 week old male C57/Bl6 mice (n=5) and minced in standard media (DMEM containing 10 % FBS and 1% penicillin/streptomycin). Minced pieces were pooled, placed into a 100 μM nylon strainer and rinsed 3 times with standard media to remove red blood cells and excess lipid. Explants were carefully removed from the top of the strainer and plated into 24-well plates. Following 48 hours of acclimatization in adipogenic medium (DMEM, 10% FBS, 1% penicillin/streptomycin, 17 nM insulin, 1 μM dexamethasone) cells were treated with adipogenic medium containing DMSO, tofacitinib or R406 at 1, 2 and 5 μM final concentrations. Each treatment was performed in triplicate. Media with fresh compound was replaced every other day. Following 7 days of treatments, RNA was extracted in Trizol (Life Technologies) following standard protocol. RT-PCR was performed using Superscript III (Life Technologies) followed by analysis on a ViiA7 Real-Time PCR System (Life Technologies). Expression was analyzed relative to 18s RNA levels. Taqman probes were purchased from Life Technologies (UCP1: catalog number Mm01244861_m1, 18S: catalog number Mm03928990_g1).

Treatment with TNFα, INFγ and cyclopamine

TNFα (human recombinant Tumor necrosis factor alpha, Sigma-Aldrich T0157) was added directly to cell medium 48 hours or 24 hours before end of assay, at a final concentration of 0.25 ng/ml or 1 ng/ml respectively. IFNγ (human recombinant Interferon-gamma, Sigma-Aldrich I3265) and cyclopamine (Tocris ,1623) were added to fresh cell medium containing DMSO, tofacitinib or R406, at day 7, 10 and 12. For all treatments, corresponding volume of solvent (PBS, DMSO or ethanol, according to supplier's recommendation) was added to control wells and used for normalization.

Gene expression analysis by branched DNA (bDNA)

Adipocytes grown in 96 well plates were collected by replacing adipocyte medium with 100 μl/well of 1× RNA lysis mixture (Panomics QuantiGene2.0 Assay kit). Lysates were transferred to mRNA capture plates containing a specific capture probe (Supplementary Table 2), incubated overnight, processed for branched DNA amplification and analyzed according to the manufacturer's instructions (Panomics QuantiGene2.0 Assay). ACTB and PPIB probes were used as housekeeping genes for normalization. Data are presented as average and standard deviation of 2 or 3 biological replicates and normalized on DMSO control.

Western blot analysis

For protein analysis, browning assays were performed in 6 well plates initially seeded with 5×10^5 PPARG2-MPCs. At differentiation day 7, PSC-WA were treated with DMSO, tofacitinib (2 μM) or R406 (1 μM) for 20 minutes and lysed in 75 ul/well of cold RIPA buffer (60 mM Tris–HCl at pH 7.4, 150 mM NaCl, 0.25% SDS, 1% NP40) containing Complete protease inhibitor (Roche) and phosphoSTOP (Roche). For browning assays over 7 days, cells were lysed in cold RIPA buffer at day 14. Western blot analysis was carried out using the following antibodies: STAT1 (Cell Signaling 9172, 1:1000), phospho-STAT1-S727 (Cell Signaling 9177, 1:1000), phospho-STAT1-Y701 (Cell Signaling 9167, 1:1000), STAT3 (Cell Signaling 4904, 1:1000), phospho-STAT3-S727 (Cell Signaling 9134, 1:1000), phospho-STAT3-Y705 (Cell Signaling 9131, 1:1000), STAT5 (Cell Signaling 9363, 1:1000), phospho-STAT5-Y694 (Cell Signaling 9351, 1:1000), Akt (Cell Signaling 4691, 1:1000), phospho-Akt-Ser473 (Cell Signaling 4060, 1:1000), Erk1/2 (Cell Signaling 9102, 1:1000), phospho-Erk1/2-Thr202/Tyr204 (Cell Signaling 4370, 1:2000), p38 MAPK (Cell Signaling 8690, 1:1000), phospho-p38-Thr180/Tyr182 (Cell Signaling 4511, 1:1000), JNK (R&D AF1387, 1:1000), phospho-JNK-T183/Y185 (R&D AF1205, 1:400), UCP1 (R&D MAB6158, 1:2000), PRDM16 (R&D AF6295, 1:200), GAPDH (SIGMA, G8795, 1:2000), COX-I (abcam 14705, 1:1000) and SDH-A (abcam 14715, 1:1000). The CHEMIDOC MP Imaging System and ImageLab Analysis Tool (BIO-RAD) or the Licor odyssey system was used to scan & quantitate the band intensity.

Reverse phase protein array (RPPA) analysis

For RPPA analysis, browning assays were performed in 10 cm dishes initially seeded with 1×10^6 PPARG2-MPCs. At differentiation day 7, adipocytes were treated with DMSO, tofacitinib (2 μM) or R406 (1 μM) for 20 minutes and lysed in 100ul of CLB1 lysis buffer. Lysates were snap-frozen in liquid nitrogen, stored at −80°C and shipped to NMI Technology Transfer GmbH (Reutlingen, Germany) for RPP analysis as follow: Lysates were printed at 4 dilutions in duplicates onto ZEPTOMARK chips (Bayer Technology Services GmbH, Leverkusen, Germany) and analyzed for 51 selected phospho-analytes. Array images were analyzed using the ZeptoVIEW 3.1 software.

Measurement of cellular Oxygen Consumption Rate (OCR)

PPARG2-MPCs and ADSCs were plated at 7×10^4 cells/well in gelatin-coated XF 24-well cell culture microplates (Seahorse Bioscience), differentiated into adipocytes at confluence and treated with DMSO, tofacitinib and R406 as described above (browning assay). Day 14 adipocytes were incubated in pre-warmed unbuffered DMEM medium (DMEM containing 2 mM GlutaMAX, 1 mM sodium pyruvate, 1.85 g l^{-1} NaCl and 25 mM glucose) for 1 h. The oxygen consumption rate was measured by the XF24 extracellular flux analyser (Seahorse Biosciences). Mitochondrial biogenesis was profiled by injecting perturbation drugs, 2 μM oligomycin, 0.5 μM CCCP (carbonyl cyanide-*p*-trifluoromethoxyphenylhydrazone) and 5 μM antimycin A, in succession. OCR were determined by plotting the oxygen tension and acidification of the medium in the chamber as a function of time and normalized by protein concentration (picomoles per minute per milligram), respectively.

Lipolysis assay

To measure lipolysis activity, DMSO, tofacitinib and R406-treated ADSC adipocytes were starved in DMEM containing 1% FBS for 1 h. Cells were then incubated in HBSS (Hank's balanced salt solution) with 2% fatty-acid-free BSA alone or with 10 μM forskolin. The culture medium was collected for glycerol measurement using the free glycerol reagent (Sigma#F6428). Protein concentrations used to normalize glycerol content were measured using the Bradford protein assay (BioRad). Glycerol release was expressed in micrograms of glycerol per milligram of total protein or the lowest value is set to 1.

RNA sequencing of adipocyte browning

A total of six, 6-well plates were prepared as follow: In each plate, three wells were seeded with PPARG2-MPC, one well with PPARG2/CEBPB/PRDM16-MPC and one well with rtTA-MPC (5×10^5 cells/well). All cells were induced and differentiated as described above. At day 7, PSC-WA received either DMSO, tofacitinib (2 μM) or R406 (1 μM). PSC-BA and MPC received DMSO only. At day 8, three cell plates were collected by adding 350 ul/well of RLT lysis buffer (Qiagen), constituting the 24h-triplicates. In the remaining three plates, treatment with DMSO, tofacitinib and R406 was repeated at day 10 and 12. At day 14, cells were collected by adding 350 ul/well of RLT lysis buffer (Qiagen), constituting the 7days-triplicates. Total RNA from adipocyte lysate was extracted and purified using the RNeasy mini kit (Qiagen) according to the manufacturer's instructions. Genomic DNA was removed from the extracted RNA using the RNase Free DNase Set (Qiagen) and purified with RNeasy Minelute Clean up Columns (Qiagen). For all samples high quality RNA was obtained (RIN between 8.1 and 9.8). RNA Sequencing libraries were prepared from 1μg of total RNA using the Illumina TruSeq RNA Sample preparation Kit v2 (Illumina) following the manufacturer's instructions. Sequencing libraries were quantified using the Kapa Library Quantification kit (Kapa Biosystems) and quality controlled by capillary electrophoresis on a Bioanalyzer using High Sensitivity chips (Agilent Technologies). Libraries were sequenced in randomized pools of three or four libraries per lane on a HiSeq2000 sequencer (Illumina) for 2× 50 cycles using version 3 cluster generation kits and version 3 sequencing reagents (Illumina). One % of PhiX control library (Illumina) was spiked into each lane as a sequencing control.

Bioinformatics and statistical analysis of RNAseq data

RNA-seq reads were first aligned to human transcriptome, and unmapped reads were then aligned to human genome. Reads that map to annotated genes were modelled by negative binomial distribution, and differential expression was quantified by generalized linear models (GLMs) implemented in the *edgeR* package. For gene-level analysis, the filter for significantly differentially expressed genes was set as |logFC|>=1 (logFC=log fold-change) and FDR<0.05 (Likelihood-ratio test, adjusted with the Benjamini-Hochberg method for multiple testing). The filtering was not necessary for gene-set-level analysis. Gene set analysis was performed with both Gene Set Enrichment Analysis (GSEA) and the CAMERA method. Gene set enrichment score (*ES*) was defined as $ES=sign(NES_{GSEA})log10(FDR_{GSEA})$, namely the sign of normalised enrichment score reported by GSEA (+1 if $NES_{GSEA}>0$, and -1 otherwise), multiplied by log10-transformed

false-discovery rate (the q-value). The enrichment score ranges between -4 and 4, corresponding to negatively or positively enriched gene sets that are statistically highly significant (FDR q<=1E-4). Gene sets in use included both pathway information from public repositories, including Reactome, StringDB and NCI-Nature pathway database, and manually curated sets of genes whose expression are regulated by upstream pathways.

General statistical analyses

Biological replicates in figure legends refer to independent adipocyte differentiation and treatment, i.e. batch-infected PPARG2-MPCs were seeded in separate wells or dishes, differentiated for 7 days in the absence of compound and matured for another 7 days in the presence of compound. Biological replicates therefore capture the biological variation of stem cell differentiation into mature adipocytes and the cellular response to compound. Repeat experiments performed with different batches of PPARG2 lentiviral particles and MPC infections are shown in Supplementary Table 3. *Technical replicates* were replicate measurements of a given sample in readout assays (bDNA, RT-PCR, lipid droplet imaging, glycerol release). Statistical analyses were carried using a two-tailed unpaired Student's t-test when $n \geq 3$ biological replicates.

Supplementary Material

Refer to Web version on PubMed Central for supplementary material.

Acknowledgements

The authors thank Inga Clausen, Martine Kapps, Roland Schmucki and Angelika Schuler for technical support, Klaus Christensen and Martin Graf for stem cell support, Laura Badi for preliminary data analysis, Corinne Solier, Annette Schell-Steven and Tobias Bergauer for experimental planning and Michael Pawlak (Natural and Medical Sciences Institute at the University of Tübingen) for RPPA analyses. A.M. was supported by the Roche Postdoctoral Fellowship (RPF) program (2011-2013). This research was supported in part by F.Hoffmann-La Roche; grant R01DK095384 (C.A.C. and Y.K.L.) and R01DK097768 (C.A.C.) from the United States Institutes of Health (NIH); and Harvard University.

REFERENCES

1. Bartelt A, et al. Brown adipose tissue activity controls triglyceride clearance. Nature medicine. 2011; 17:200–205.
2. Stanford KI, et al. Brown adipose tissue regulates glucose homeostasis and insulin sensitivity. The Journal of clinical investigation. 2013; 123:215–223. [PubMed: 23221344]
3. Cypess AM, et al. Identification and importance of brown adipose tissue in adult humans. The New England journal of medicine. 2009; 360:1509–1517. [PubMed: 19357406]
4. Ghorbani M, Himms-Hagen J. Appearance of brown adipocytes in white adipose tissue during CL 316,243-induced reversal of obesity and diabetes in Zucker fa/fa rats. International journal of obesity and related metabolic disorders : journal of the International Association for the Study of Obesity. 1997; 21:465–475.
5. Granneman JG, Li P, Zhu Z, Lu Y. Metabolic and cellular plasticity in white adipose tissue I: effects of beta3-adrenergic receptor activation. American journal of physiology. Endocrinology and metabolism. 2005; 289:E608–616. [PubMed: 15941787]
6. Himms-Hagen J, et al. Multilocular fat cells in WAT of CL-316243-treated rats derive directly from white adipocytes. American journal of physiology. Cell physiology. 2000; 279:C670–681. [PubMed: 10942717]

7. Li P, Zhu Z, Lu Y, Granneman JG. Metabolic and cellular plasticity in white adipose tissue II: role of peroxisome proliferator-activated receptor-alpha. American journal of physiology. Endocrinology and metabolism. 2005; 289:E617–626. [PubMed: 15941786]
8. Koh YJ, et al. Activation of PPAR gamma induces profound multilocularization of adipocytes in adult mouse white adipose tissues. Experimental & molecular medicine. 2009; 41:880–895. [PubMed: 19745605]
9. Murano I, Barbatelli G, Giordano A, Cinti S. Noradrenergic parenchymal nerve fiber branching after cold acclimatisation correlates with brown adipocyte density in mouse adipose organ. Journal of anatomy. 2009; 214:171–178. [PubMed: 19018882]
10. Petrovic N, et al. Chronic peroxisome proliferator-activated receptor gamma (PPARgamma) activation of epididymally derived white adipocyte cultures reveals a population of thermogenically competent, UCP1-containing adipocytes molecularly distinct from classic brown adipocytes. The Journal of biological chemistry. 2010; 285:7153–7164. [PubMed: 20028987]
11. Wu J, et al. Beige adipocytes are a distinct type of thermogenic fat cell in mouse and human. Cell. 2012; 150:366–376. [PubMed: 22796012]
12. Rosenwald M, Perdikari A, Rulicke T, Wolfrum C. Bi-directional interconversion of brite and white adipocytes. Nature cell biology. 2013; 15:659–667.
13. van der Lans AA, et al. Cold acclimation recruits human brown fat and increases nonshivering thermogenesis. The Journal of clinical investigation. 2013; 123:3395–3403. [PubMed: 23867626]
14. Yoneshiro T, et al. Recruited brown adipose tissue as an antiobesity agent in humans. The Journal of clinical investigation. 2013; 123:3404–3408. [PubMed: 23867622]
15. Ahfeldt T, et al. Programming human pluripotent stem cells into white and brown adipocytes. Nature cell biology. 2012; 14:209–219.
16. Bonet ML, Oliver P, Palou A. Pharmacological and nutritional agents promoting browning of white adipose tissue. Biochimica et biophysica acta. 2013; 1831:969–985. [PubMed: 23246573]
17. Kozak UC, et al. An upstream enhancer regulating brown-fat-specific expression of the mitochondrial uncoupling protein gene. Molecular and cellular biology. 1994; 14:59–67. [PubMed: 8264627]
18. Rubio A, Raasmaja A, Maia AL, Kim KR, Silva JE. Effects of thyroid hormone on norepinephrine signaling in brown adipose tissue. I. Beta 1- and beta 2-adrenergic receptors and cyclic adenosine 3′,5′-monophosphate generation. Endocrinology. 1995; 136:3267–3276. [PubMed: 7628360]
19. Rubio A, Raasmaja A, Silva JE. Thyroid hormone and norepinephrine signaling in brown adipose tissue. II: Differential effects of thyroid hormone on beta 3-adrenergic receptors in brown and white adipose tissue. Endocrinology. 1995; 136:3277–3284. [PubMed: 7628361]
20. Rabelo R, Schifman A, Rubio A, Sheng X, Silva JE. Delineation of thyroid hormone-responsive sequences within a critical enhancer in the rat uncoupling protein gene. Endocrinology. 1995; 136:1003–1013. [PubMed: 7867554]
21. Mocsai A, Ruland J, Tybulewicz VL. The SYK tyrosine kinase: a crucial player in diverse biological functions. Nature reviews. Immunology. 2010; 10:387–402.
22. Richard AJ, Stephens JM. The role of JAK-STAT signaling in adipose tissue function. Biochimica et biophysica acta. 2014; 1842:431–439. [PubMed: 23735217]
23. Meyer DM, et al. Anti-inflammatory activity and neutrophil reductions mediated by the JAK1/JAK3 inhibitor, CP-690,550, in rat adjuvant-induced arthritis. Journal of inflammation. 2010; 7:41. [PubMed: 20701804]
24. Flanagan ME, et al. Discovery of CP-690,550: a potent and selective Janus kinase (JAK) inhibitor for the treatment of autoimmune diseases and organ transplant rejection. Journal of medicinal chemistry. 2010; 53:8468–8484. [PubMed: 21105711]
25. Braselmann S, et al. R406, an orally available spleen tyrosine kinase inhibitor blocks fc receptor signaling and reduces immune complex-mediated inflammation. The Journal of pharmacology and experimental therapeutics. 2006; 319:998–1008. [PubMed: 16946104]
26. Cao W, Medvedev AV, Daniel KW, Collins S. beta-Adrenergic activation of p38 MAP kinase in adipocytes: cAMP induction of the uncoupling protein 1 (UCP1) gene requires p38 MAP kinase. The Journal of biological chemistry. 2001; 276:27077–27082. [PubMed: 11369767]

27. Cao W, et al. p38 mitogen-activated protein kinase is the central regulator of cyclic AMP-dependent transcription of the brown fat uncoupling protein 1 gene. Molecular and cellular biology. 2004; 24:3057–3067. [PubMed: 15024092]

28. Valladares A, Roncero C, Benito M, Porras A. TNF-alpha inhibits UCP-1 expression in brown adipocytes via ERKs. Opposite effect of p38MAPK. FEBS letters. 2001; 493:6–11. [PubMed: 11277995]

29. Aaronson DS, Horvath CM. A road map for those who don't know JAK-STAT. Science. 2002; 296:1653–1655. [PubMed: 12040185]

30. Todoric J, et al. Cross-talk between interferon-gamma and hedgehog signaling regulates adipogenesis. Diabetes. 2011; 60:1668–1676. [PubMed: 21536945]

31. Pospisilik JA, et al. Drosophila genome-wide obesity screen reveals hedgehog as a determinant of brown versus white adipose cell fate. Cell. 2010; 140:148–160. [PubMed: 20074523]

32. Derecka M, et al. Tyk2 and Stat3 regulate brown adipose tissue differentiation and obesity. Cell metabolism. 2012; 16:814–824. [PubMed: 23217260]

15. Ahfeldt T, et al. Programming human pluripotent stem cells into white and brown adipocytes. Nature cell biology. 2012; 14:209–219.

34. Bray, MA.; Carpenter, A. Advanced Assay Development Guidelines for Image-Based High Content Screening and Analysis. In: Sittampalam, GS., et al., editors. Assay Guidance Manual. Bethesda (MD): 2004.

35. Prummer M. Hypothesis testing in high-throughput screening for drug discovery. Journal of biomolecular screening. 2012; 17:519–529. [PubMed: 22233646]

36. Storey JD. A direct approach to false discovery rates. Journal of the Royal Statistical Society: Series B (Statistical Methodology). 2002; 64:479–498.

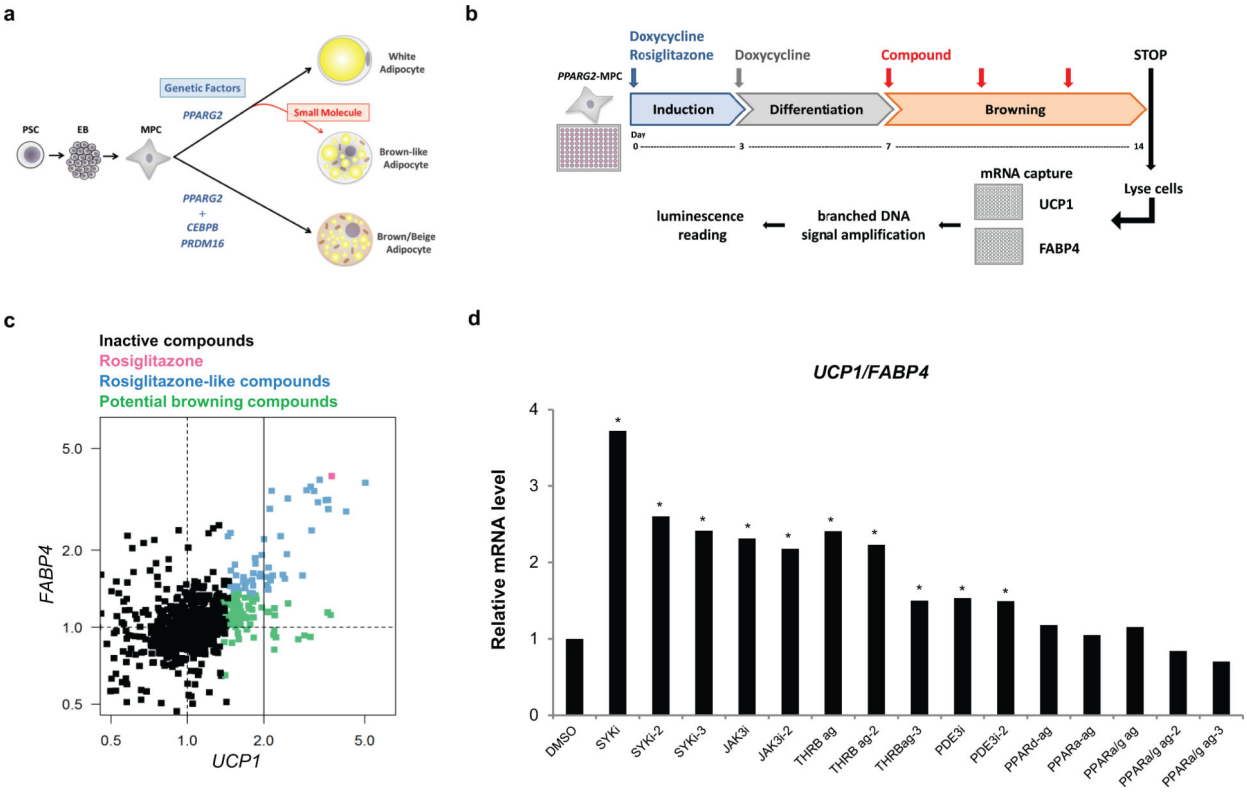

Figure 1. Browning screen in human stem cell-derived adipocytes

a) Conceptual strategy to identify small molecules with adipocyte browning effect using human stem cells. PSC: pluripotent stem cells, EB: embryoid bodies, MPC: mesenchymal progenitor cells.

b) Adipocyte browning screen, assay workflow. *PPARG2* expressing-MPC (PPARG2-MPC) were maintained in adipogenic medium containing doxycycline and rosiglitazone for 3 days in order to induce adipogenesis, and differentiated in the absence of rosiglitazone for 4 days. A library of 867 compounds of known mode of action was applied to PSC-WA at day 7, 10 and 12. Total mRNA was collected at day 14, and *UCP1* and *FABP4* mRNA levels were quantified using the branched DNA technology. PPARG2-MPC: mesenchymal progenitor cells transduced with rtTA and doxycycline-inducible *PPARG2* expression vectors. For more details see the methods section.

c) Scatter plot display of browning screen results. Each data point represents the average of two biological replicates per compound, normalized on DMSO control. X axis: *UCP1* mRNA level as an indicator of adipocyte browning, Y axis: *FABP4* mRNA as an indicator of general adipogenesis. The color code distinguishes inactive compounds (black) from active ones: Rosiglitazone (red), Rosiglitazone-like compounds that increase *UCP1* and *FABP4* (blue), and potential browning compounds that induce *UCP1* specifically (green). Dashed lines indicate neutral conditions, solid line delineates *UCP1* induction above 2 fold.

d) Validation of browning hits by bDNA analysis showing that JAK3 inhibitors, SYK inhibitors and THRB agonists scored as best *UCP1/FABP4* inducers. All compounds were added at a 5 μM final concentration. X axis: Compounds are identified by target and mode

of action. i= inhibitor, ag = agonist. For chemical nomenclature see the methods section. Values represent the mean of two biological replicates.

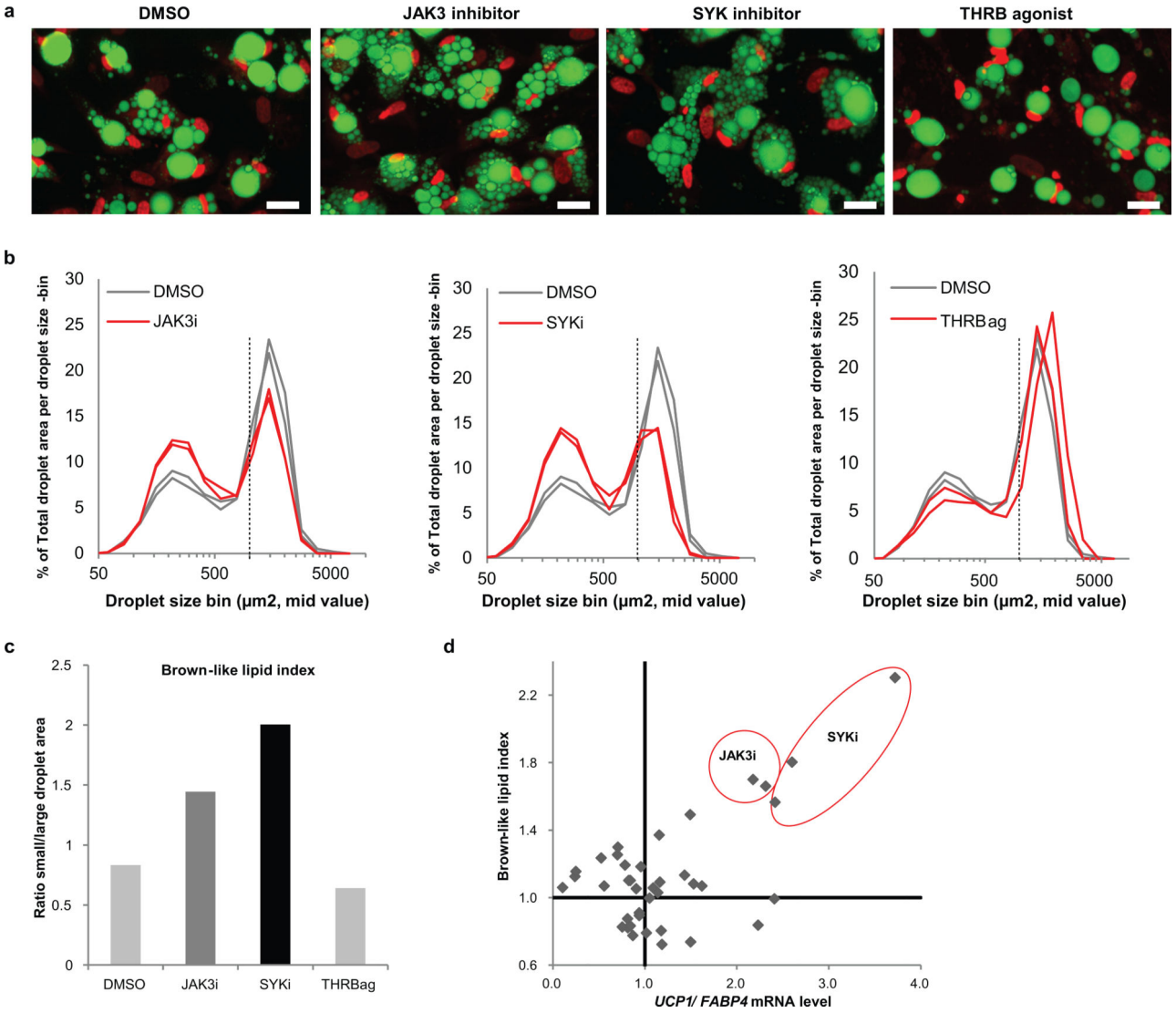

Figure 2. Selected compounds modulate lipid morphology

a) PSC-WA were differentiated and treated as described in Fig1B. At day 14, cells were fixed, stained and imaged by confocal microscopy. Green: lipids, Red: nuclei. Scale bars, 50µm. Images are representative of n =3 biological replicates.

b) Quantification of changes in lipid morphology is depicted as fraction of total lipid area (Y axis) per lipid droplet size (X axis). JAK3 inhibitor, SYK inhibitor and THRB agonist-treated cells are shown in red and DMSO in gray. Values represent the mean of two biological replicates.

c) Bar graph illustrating the quantification of a brown-like lipid index, determined by calculating the ratio of total area for small (<1070µm^2) versus large (>1070µm^2) lipid droplets for the graphs in b), normalized to the DMSO control sample. Values represent the mean of two biological replicates.

d) Scatter plot showing the relation between *UCP1*/*FABP4* mRNA (X axis) and brown-like lipid morphology (Y axis) upon treatment with 39 selected compounds. Brown-like lipid

index refers to the ratio of small/large lipid droplets normalized on DMSO as determined in b). Values represent the mean of two biological replicates.

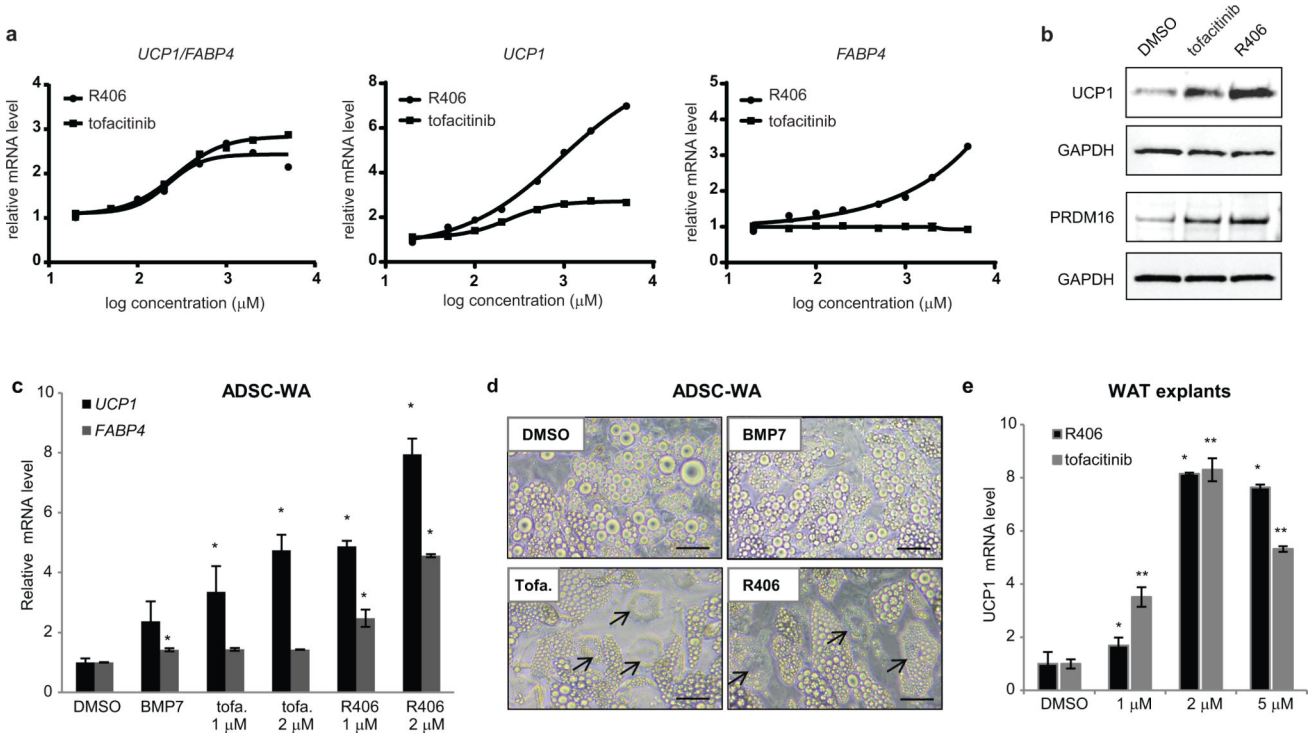

Figure 3. Validation of tofacitinib and R406 browning compounds in primary adipocytes

a) bDNA analysis of dose response with tofacitinib and R406. At high doses, R406 increases both *UCP1* and *FABP4* expression but *UCP1*/*FABP4* remains above 2. Values represent the mean of two biological replicates.

b) Western blot analysis showing that up-regulation of *UCP1* and PRDM16 protein levels correlates with up-regulation of *UCP1* mRNA by tofacitinib and R406.

c) bDNA analysis showing that tofacitinib (tofa.) and R406 increase *UCP1* expression in human primary adipocytes. ADSC: Adipose tissue-derived stromal cells. Values are mean ± s.d. of n = three biological replicates and differences from DMSO are significant for * $P < 0.05$. *P* values were calculated using the two-tailed paired Student's t-test.

d) Bright field images showing that tofacitinib (tofa.) and R406 induce brown-like lipid morphology (arrows) in human primary adipocytes more prominently than BMP7. ADSC: Adipose tissue-derived stromal cells. Scale bars, 20μm. Data representative of 3 independent experiments. For uncropped images see Supplementary Figure 3.

e) RT-PCR analysis of *UCP1* gene expression in mouse subcutaneous white adipose tissue (WAT) explants following 7 days of treatment with the indicated compound. Values are mean ± S.E.M. of n = three biological replicates of pooled tissue from 5 mice and differences from DMSO are significant for * $P < 0.05$ and ** $P < 0.005$. *P* values were calculated using the two-tailed paired Student's t-test.

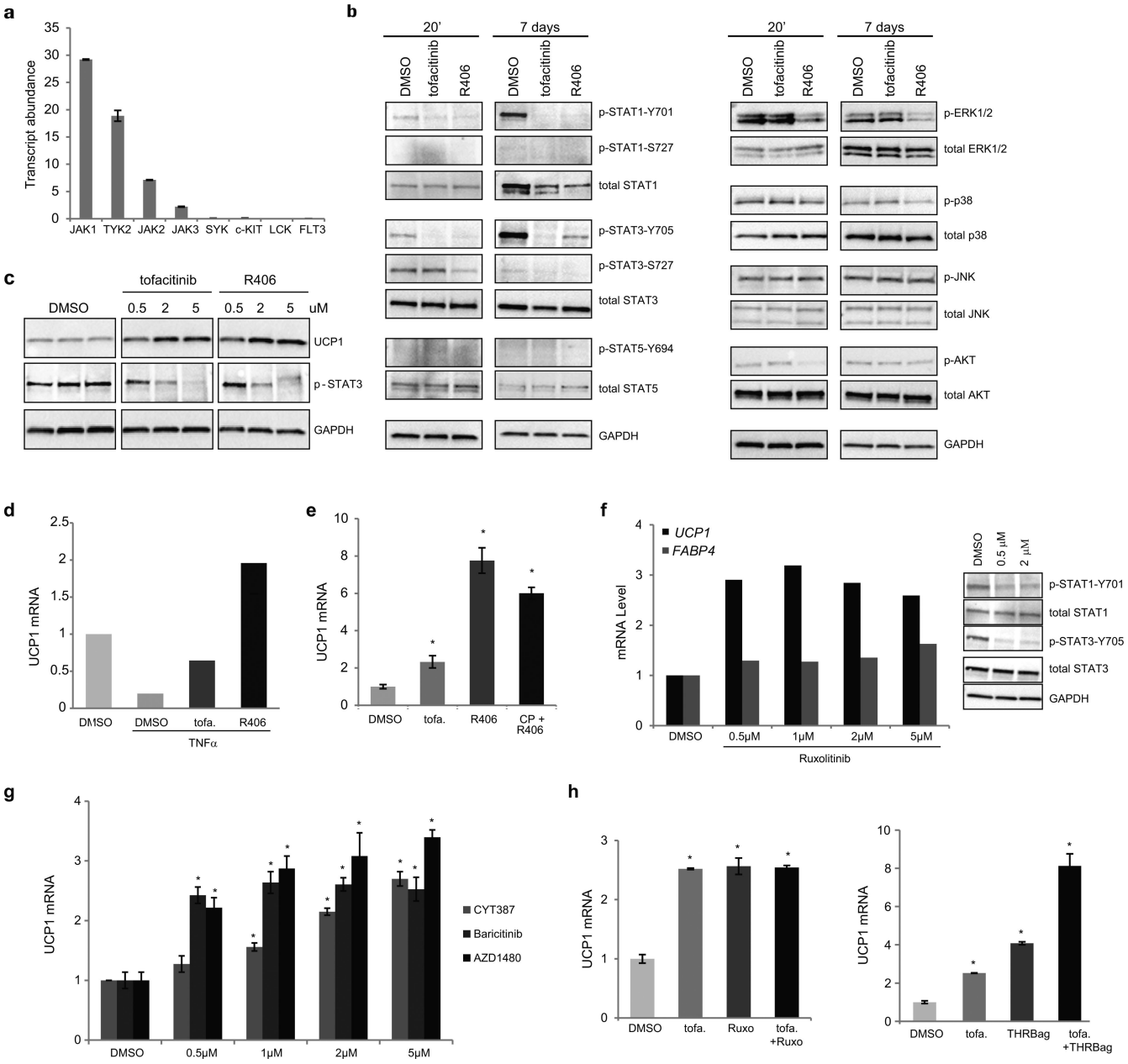

Figure 4. Inhibition of STAT phosphorylation downstream of tofacitinib and R406

a) Transcript abundance in RPKM (reads per kilobase transcript per million reads) of known targets of tofacitinib and R406 indicating that the JAK kinases are predominantly represented in PSC-WA. Values are mean ± s.d. of n = three biological replicates.

b) Western blot analyses of STATs, AKT and MAPKs in PSC-WA previously treated with DMSO, tofacitinib and R406 for 20 minutes or 7 days showing a pronounced inhibition of STAT phosphorylation by tofacitinib and R406 at both time points. R406 also significantly decreased phosphorylation levels of AKT and ERK1/2. The data shown is representative of two independent experiments.

c) Western blot analysis of a dose-response with tofacitinib and R406 showing the correlation between UCP1 accumulation and inhibition of STAT3 phosphorylation. The data shown is representative of two independent experiments.

e) bDNA analysis of PSC-WA differentiated as in figure 1b) and treated with TNFα at day 12, indicating that the negative effect of TNFα on *UCP1* expression is rescued by tofacitinib and R406. Values represent the mean of two biological replicates.

f) Tofacitinib (tofa.) and R406 do not synergize during adipocyte browning. PSC-WA were treated with tofacitinib, R406 or a combination of both and analyzed for *UCP1* expression by bDNA. Values are mean ± s.d. of n = three biological replicates and differences from DMSO are significant for * $P < 0.05$. *P* values were calculated using the two-tailed paired Student's t-test.

d) The JAK 1/2 inhibitor Ruxolitinib positively modulates *UCP1* expression (graph) and inhibits STAT1/3 phosphorylation (right panels) in PSC-WA. Graph values of bDNA analysis represent the mean of two biological replicates. Images of western blot analysis are representative of two independent experiments.

g) bDNA analysis showing that the JAK1/2 inhibitors CYT387, AZD1480 and Baricitinib positively regulate *UCP1* expression in PSC-WA. Values are mean ± s.d. of n = three biological replicates and differences from DMSO are significant for * $P < 0.005$. *P* values were calculated using the two-tailed paired Student's t-test.

h) Tofacitinib (tofa.) synergizes with THRB agonist (right panel) but not with Ruxolitinib (Ruxo., left panel) during adipocyte browning. Values are mean ± s.d. of n = three biological replicates and differences from DMSO are significant for * $P < 0.005$. *P* values were calculated using the two-tailed paired Student's t-test.

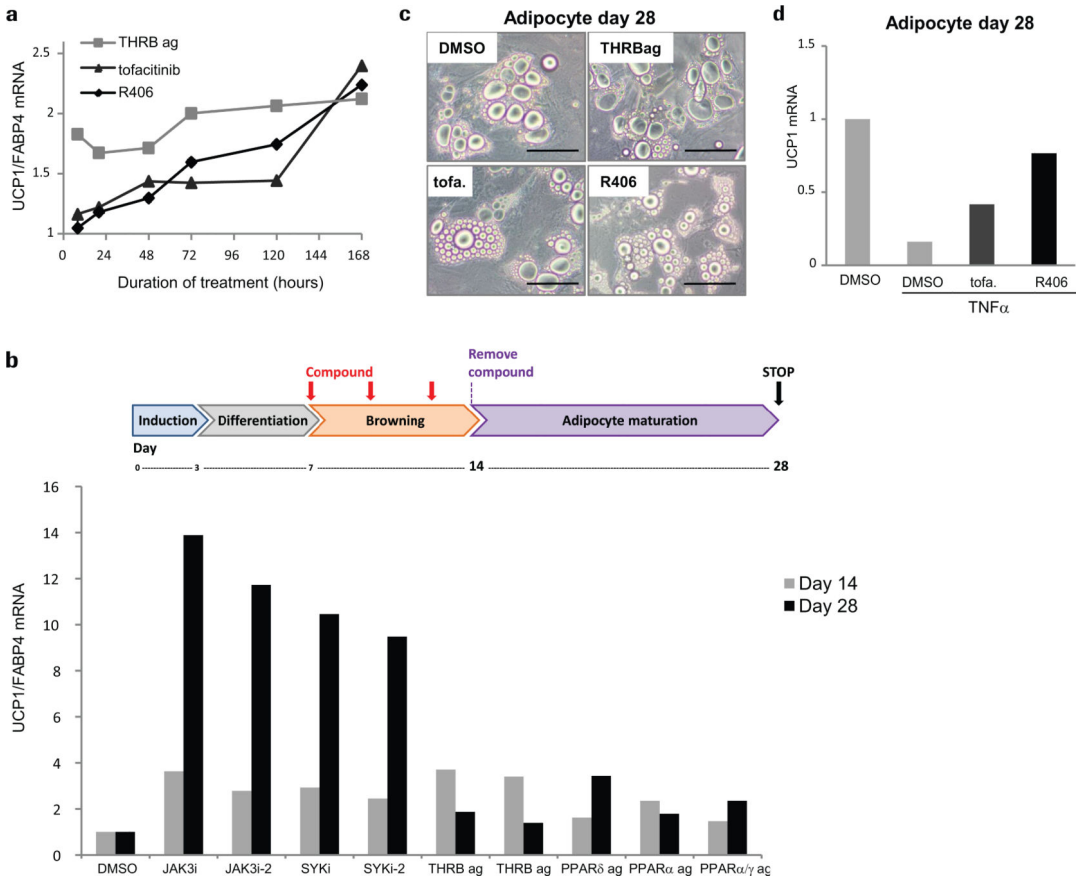

Figure 5. JAK inhibition stably induces a brown-like profile in adipocytes

a) bDNA quantification of *UCP1* mRNA levels over time, showing that the progressive accumulation of *UCP1* induced by tofacitinib and R406 contrasts with the acute effect of THRB agonists. Values represent the mean of two biological replicates.

b) Schematic illustration of experimental design for b), c), and d): PSC-WA were treated with compounds for 7 days, washed 3 times with compound-free medium, and maintained in compound-free medium for an additional 14 day-period. Images were captured at day 28 prior to addition of lysis buffer and bDNA analysis. Only JAK3i and SYKi-pre-treated cells displayed high levels of *UCP1* mRNA relative to DMSO. Values represent the mean of two biological replicates.

c) Bright field images showing a reduced lipid vacuole size at day 28 for tofacitinib (tofa.) and R406-pre-treated adipocytes. Scale bars, 50μm. Images are representative of two independent experiments.

d) DMSO, tofacitinib (tofa.) and R406-pre-treated adipocytes were exposed to TNFα from day 26 to 28. bDNA analysis shows that pre-treatment with tofacitinib and R406 protects adipocytes from TNFα-mediated down-regulation of *UCP1* expression. Values represent the mean of two biological replicates.

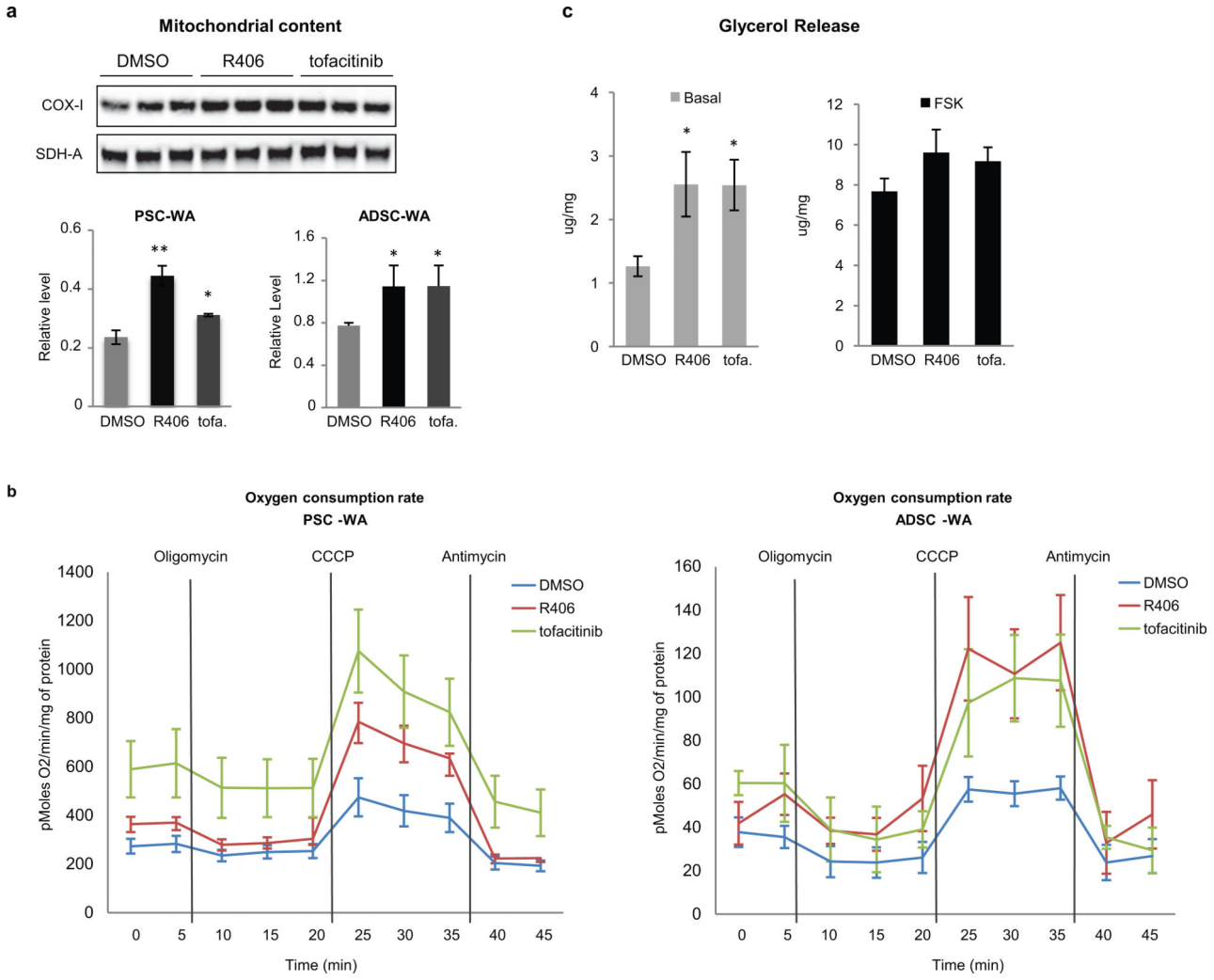

Figure 6. JAK inhibition induces brown-like metabolic properties in adipocytes

a) Mitochondrial content was assessed by determining the ratio of COX-I on SDH-A protein levels by immunoblots as shown in upper panel for PSC-WA. Quantification of immunoblots revealed up-regulation of mitochondrial content in tofacitinib and R406-treated PSC-WA and ADSC adipocytes. Values are mean ± s.e.m. of n = three biological replicates and differences from DMSO are significant for * $P < 0.05$ and ** $P < 0.01$. P values were calculated using the two-tailed paired Student's t-test.

b) Tofacitinib and R406-treated PSC-WA and ADSC adipocytes have higher oxygen consumption rate (OCR) compare to DMSO-treated adipocytes. Values are mean ± s.e.m. of n = four (DMSO and tofacitinib) and n = three (R406) biological replicates.

c) The degree of lipolytic activity was assessed by quantification of glycerol release. tofacitinib (tofa.) and R406-treated ADSC adipocytes showed increased lipolysis in the basal state (upper graph), but no in Forskolin (FSK)-stimulated cells (lower graph. Values are mean ± s.e.m. of n = three biological replicates and differences from DMSO are significant for * $P < 0.05$. P values were calculated using the two-tailed paired Student's t-test.

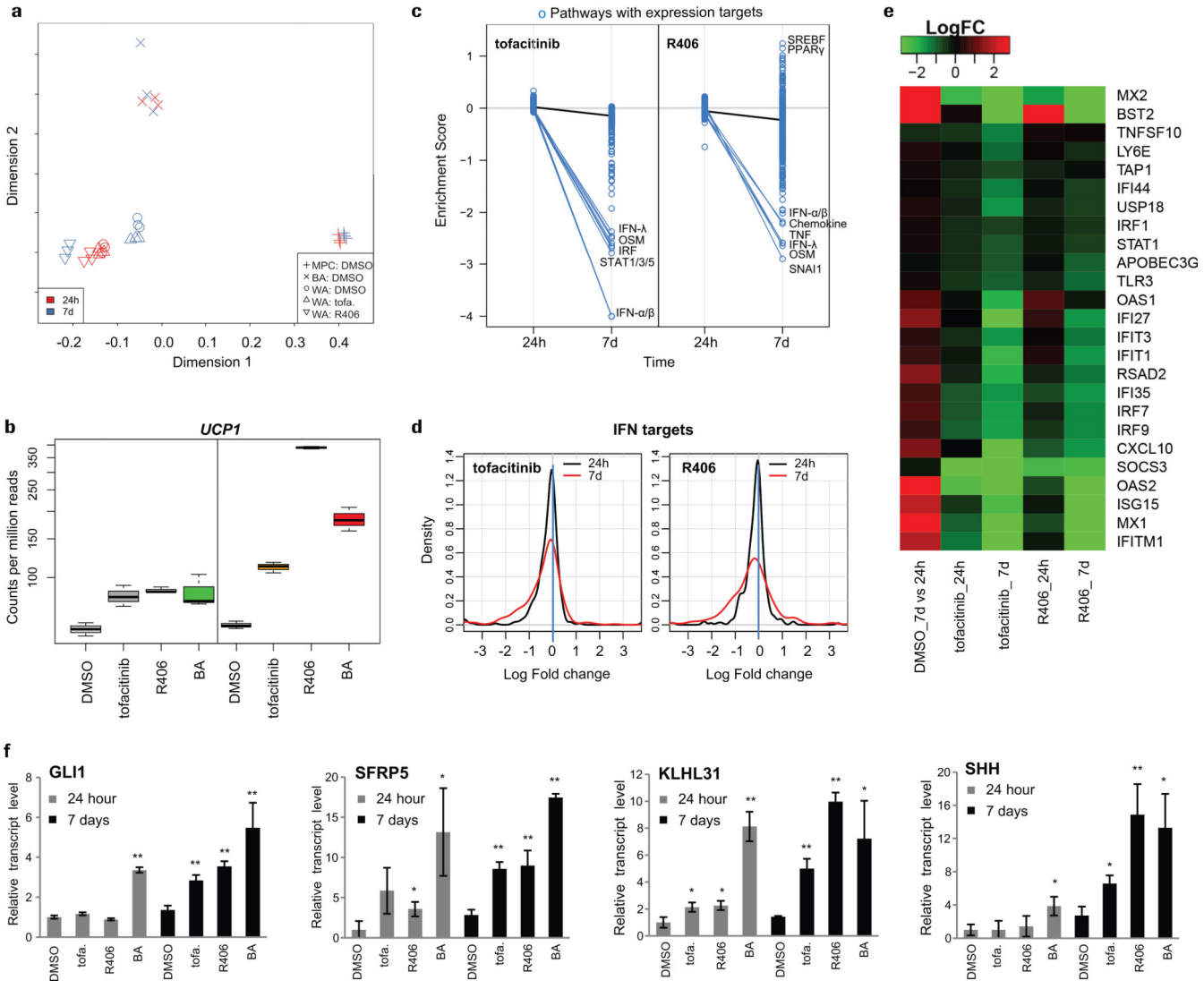

Figure 7. Gene signature and cellular identity of JAK-inactivated adipocytes

a-f) Adipocytes were differentiated according to scheme 1B, treated with tofacitinib and R406 at day 7, and collected at day 8 (24h time point) or day 14 (d7 time point). N= 3 biological replicates. Each independent biological replicate was pooled from two individual wells.

a) Multi-dimensional scaling of RNA sequencing data revealing the white lineage identity of tofacitinib (tofa.) and R406 treated PSC-WA.

b) Levels of *UCP1* transcripts served as experimental control for adipocyte browning. *UCP1* transcripts are higher in BA versus WA and higher in tofacitinib (tofa.) and R406-treated PSC-WA compare to DMSO-treated PSC-WA.

c) Interferon targets and pro-inflammatory pathways are significantly down-regulated by both compounds at 7d in PSC-WA. Enrichment scores of 9116 gene sets are compared between two time points (24h and 7d) for both compounds. Each circle represents one gene set that is coherently regulated by an upstream pathway. Black lines indicate the change of

average scores, and blue lines the change of individual pathways that are significantly reduced (|ΔES|>=2).

d) Differential expression profiles of interferon targets induced by tofacitinib and R406. A substantial subset of target genes are negatively regulated in both cases, making the density curves of logFC shifts toward left and thereby forming a “red shoulder”. Compared with 24h, the expression of interferon pathway targets are repressed by both compounds at 7d (*P* =2.94E-6 and 2.06E-5, respectively; one-sided Kolmogorov-Smirnov test).

e) Differential expression profiles of selected interferon target genes in heatmap.

f) Whole transcriptome analysis revealed that the sonic hedgehog responsive genes GLI1, SFRP5, KLHL31 and SHH were up-regulated in tofacitinib (tofa.) and R406-treated adipocytes at day 7 compare to DMSO control. Values are mean ± s.d. of n = three biological replicates and differences from DMSO are significant for * $P < 0.05$ and ** $P < 0.01$. *P* values were calculated using the two-tailed paired Student's t-test.

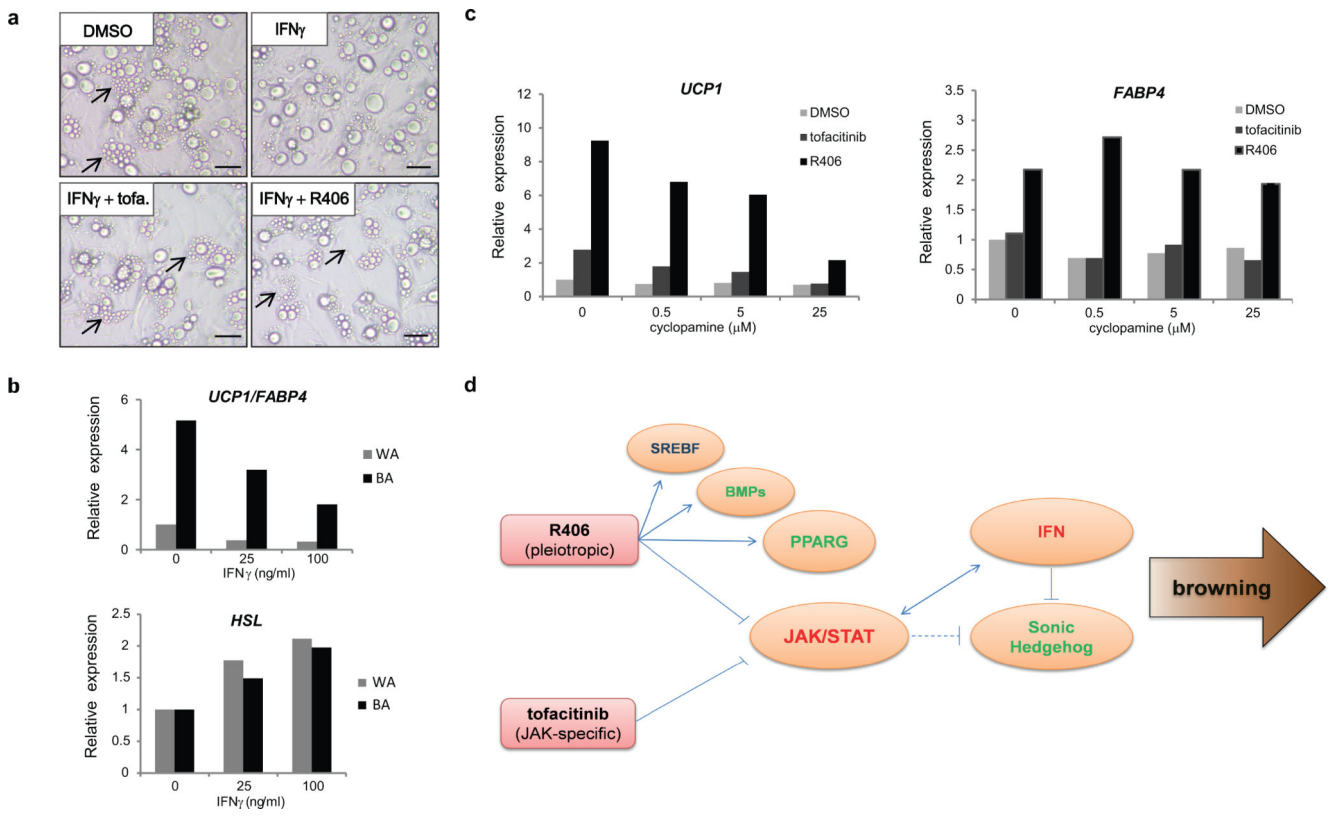

Figure 8. IFN and SHH signaling contribute to adipocyte browning downstream of JAK inhibition

a) Whitening of IFNγ-treated adipocytes is visible as lipid accumulation forms a single, large vacuole. Treatment with tofacitinib (tofa.) and R406 restores the formation of small lipid droplets (arrows). Bright field images representative of two independent experiments. Scale bars, 20μm.

b) IFNγ treatment decreases the *UCP1*/*FABP4* ratio (upper graph) and increases the expression of HSL, a marker of white adipocyte (lower graph) both in WA and BA. Values represent the mean of two biological replicates.

c) The SHH pathway antagonist cyclopamine fully blocks CP-6990550-mediated browning as judged by *UCP1* level and partially blocks SYKi-mediated browning (left graph). Cyclopamine didn't restore R406-induced *FABP4* levels, thereby decoupling the regulation of *UCP1* and *FABP4* by R406 (right graph). Values represent the mean of two biological replicates.

d) Model of adipocyte browning by pharmacological inhibition of JAK. Tofacitinib and R406 inhibit the JAK-STAT pathway in human adipocytes, leading to down-regulation of the interferon alpha, beta and gamma responses. Sustained shut down of IFN signaling relieves inhibition of the sonic hedgehog (SHH) pathway and thereby contributes to accumulation of *UCP1*. R406 acts as a pleiotropic drug with broad effects on adipocytes through activation of PPARG, BMPs and SREBF target genes. Red fonts: negative regulator of browning; Green fonts: positive regulator of browning; Arrows: activation; Flat lines: inhibition; Dash lines: hypothetical.